

A comparison of cortical and trabecular bone from C57 Black 6 mice using Raman spectroscopy

Simon R Goodyear¹, Iain R Gibson^{2, 3}, Janet M S Skakle³, Richard P K Wells³, Richard M Aspden¹

¹ Bone and Musculoskeletal Programme, Division of Applied Medicine, University of Aberdeen, United Kingdom

² School of Medical Sciences, University of Aberdeen, United Kingdom

³ Department of Chemistry, University of Aberdeen, United Kingdom

Corresponding Author: Simon R Goodyear

Address: Bone and Musculoskeletal Programme
Division of Applied Medicine
University of Aberdeen
IMS 2.26
Foresterhill
Aberdeen
AB25 2ZD

Telephone Number: +44 (0)1224 554910

Fax Number: +44 (0)1224 559533

Email address: s.goodyear@abdn.ac.uk

Abstract

Cortical and trabecular bone are both produced and maintained by the same cell types. At the microscopic scale they have a similar lamellar structure but at a macroscopic scale they are very different. Raman microscopy has been used to investigate compositional differences in the two bone types using bone from standard laboratory mice in physiological conditions. Clear differences were observed when complete spectra were compared by principal component analysis (PCA). Analysis of individual bands showed cortical bone to have compositional characteristics of older bone when compared with trabecular material, possibly due to the higher bone turnover traditionally reported in the trabecular compartment.

Keywords

Cortical bone, trabecular bone, mouse, Raman spectroscopy, composition

Introduction

The mammalian skeleton contains two different forms of bone, cortical and trabecular. Cortical, or compact, bone is found mainly in the shafts of long bones and accounts for roughly 80% of bone mass [1]. Trabecular bone is found in vertebrae and the ends of long bones and is, in contrast, a porous foam-like structure with voids filled with bone marrow. Both bone types are created by osteoblasts and resorbed by osteoclasts, and the controlled interaction of both cell types enables bone growth during development and damage repair at maturity to maintain mechanical strength. A hierarchy of structures can be seen in cortical and trabecular bone at successively smaller length scales (see e.g. [1,2] for further details). At the macroscopic scale bone types appear vastly different with cortical bone comprising cylindrical osteons (in mice the osteonal structure is not present and the cortex resembles a “super osteon” as bone is not remodelled, probably because of its small size compared to osteoclasts and osteoblasts [3]) and trabecular bone forming a lattice of plates and rods. In contrast, both bone types appear very similar at the molecular scale, being composed of mineralised collagen fibrils laid down with a preferred orientation in lamellae. Trabecular bone with its large surface area is more metabolically active than cortical bone [4] and is the type of bone in which the quickest response to external factors is seen. For instance, studies have shown athletic training in rodents [5] and man [6], ovariectomy [7], cathepsin K overexpression [8] and parathyroid hormone deficiency and excess [9] have a more immediate effect in trabecular bone. In osteoporosis, a major disease of bone, fractures occur mostly in the hip, wrist and spine, areas with a high trabecular bone content [10].

A number of studies have examined cortical and trabecular bone types using a variety of methods. Gong et al. compared their compositions in mammals by ashing and found that ash to organic fraction ratios were higher in cortical bone [11]; although cortical and trabecular samples were taken from different anatomical sites in the animal and it is not clear how much

of the difference could be a site variation. Differences in the mineral content have been measured in whole bone by micro-computed tomography [12] and X-ray diffraction, infra-red (IR) spectroscopy and chemical means [13]. Both of these studies showed cortical bone to be more mineralised than trabecular bone. A chemical technique, used to measure collagen cross-linking in demineralised bone, showed cortical material to have more mature, pyridinium type cross-links than trabecular bone [14]. The elastic properties of both bone types have been measured using nanoindentation [15,16], acoustic microscopy [17] or both [18], or back-calculated by comparing experimental results with finite element predictions [19]. Generally, cortical bone has been found to have a greater modulus than trabecular material. The picture is clouded, however, by orientation effects, with cortical bone being stiffer longitudinally than transversely. To date the transverse modulus in a single trabecula has not been measured because of difficulties due to its small size.

Raman microscopy provides a powerful way of determining the chemical properties of materials with a spatial resolution approaching a micrometre. In bone this enables the study of biologically relevant locations, structures and process on this scale, often difficult with Fourier-transform infra-red spectroscopy (FTIR) because of the inferior resolution associated with this technique [20-24]. As Raman is a scattering phenomenon it can be used in reflection mode on solid samples. In contrast to FTIR, this technique is relatively insensitive to water, allowing the analysis of fully hydrated samples, and its non-destructive nature means the same sample can be examined using a variety of different techniques. A further advantage is that it can simultaneously measure organic and mineral phases. The Raman signal, however, depends not only on the composition but also the local orientation of fibres or crystals with respect to a polarised illuminating source, making interpretation of spectra from bone more complicated than from isotropic materials. Previous studies have used Raman microspectroscopy to compare bone from wild type and knock out animals to determine the

effect of particular genes on bone e.g. [25,26], and to monitor the process of mineralisation in osteoblasts over time both in vitro [27] and in vivo [28]. The effect of aging has been investigated by observing changes in collagen band positions [29,30]. Lamellae in osteons have been mapped by observing changes in the magnitude of the Amide I band [31] or from measurements in two orthogonal planes in cortical bone [32]. Although cortical and trabecular bone have been studied separately, there appears to have been no direct comparison between them from closely related sites in the same animals. This study used Raman microscopy to compare cortical and trabecular bone tissue from the same femur and tibia of standard laboratory mice, C57 Black 6 (C57Bl6). To keep the bones in their physiological condition, sample preparation was kept to a minimum and was restricted to soft tissue removal and cutting to expose the cross section.

Materials and Methods

Materials

Cortical and trabecular samples were taken from the distal femur and proximal tibia from ten 5-month-old, male, C57Bl6 mice. The bones had previously been broken in a 3-point bending test and, because of difficulties holding the relevant section for cutting, samples were obtained from 5 of the tibiae only. Skeletal maturity in terms of mechanical properties is reached at about 4 months [33]. Following soft tissue removal, 1.5 mm long transverse sections were cut using a mineralogical saw (Accutom 2, Struers, Glasgow) fitted with an aluminium oxide cut-off wheel under constant irrigation with distilled water. Slices were then glued to a microscope slide with cyanoacrylate adhesive (Loctite) for acquiring spectra. Slides were kept submerged in phosphate buffered saline (PBS) prior to and during testing.

Raman microscopy

A Renishaw inVia microscope (Renishaw plc, Gloucestershire, UK) fitted with a 300 mW, 785 nm laser and x63/0.95 numerical aperture Achromplan immersion objective lens (Zeiss) was used to acquire spectra from the submerged bone samples. At the beginning of each imaging session the laser was checked for alignment with the optical axis of the microscope and the wavenumber datum verified against a silicon internal standard. Care was also taken to ensure that the silicon band intensity was the same each time, thus ensuring comparability of spectral intensities. Data were recorded between 300 and 1800 cm^{-1} at a resolution of better than 4 cm^{-1} . Between 10 and 40 spectra were recorded from random sites on each sample. Each spectrum was the result of 10 accumulations each with a 10 second exposure time. The spectra from each bone sample were averaged to give a representative spectrum for that bone. In cortical regions spectra were taken at spots around the whole circumference of the bone and averaged, effectively removing any orientation effect due to the preferred orientation of either collagen or apatite and the polarisation vector of the incident laser beam. Spectra from trabecular bone were acquired from a number of locations within the field of view however the orientation of lamellae could not be discerned so it is possible some orientation bias remained after averaging.

Preprocessing

Cosmic ray artefacts were removed manually from each spectrum using WIRE 2.0 software (Renishaw plc, Gloucestershire, UK). Noise was removed using a wavelet technique [34,35] and the underlying background signal subtracted from each spectrum using an iteratively fitted polynomial [36]. Preprocessing was performed using custom written procedures in Matlab (the Mathworks, Inc., Natick, MA, USA). Both peak heights and peak areas were

calculated but the analysis showed no difference in the results. We chose then to present only the heights as these were simpler to derive, and there is precedence in the literature {{}}. Spectra were then analysed in 3 different ways: by direct comparison between spectra from cortical and trabecular bone, by comparison of parameters derived from peak intensities and, finally, using principal components analysis (PCA). At no point were the spectra normalised.

Difference spectra

Average spectra were calculated for each bone type by summing all the spectra (e.g. for trabecular bone) and dividing by the number of spectra for that type of bone. A difference spectrum was found by subtracting the intensity of the trabecular spectrum from the cortical spectrum at each wave number. The significance of any difference was determined by comparing the average spectra from cortical and trabecular bone using Student's *t*-test.

Peak Parameters

A typical spectrum from bone is shown in Figure 1 with the relevant band assignments marked. The band at 961 cm^{-1} corresponds to the symmetric stretching vibration (ν_1) of the phosphate ion and is the strongest marker of bone mineral. The phosphate bending vibrations ν_2 and ν_4 appear at 438 cm^{-1} and 589 cm^{-1} respectively while the non symmetric stretch (ν_3) causes a band at about 1040 cm^{-1} . A peak due to a superposition of carbonate and phosphate ν_3 appears at 1070 cm^{-1} . The high frequency peaks arise from the organic phase and these are the amide III ($\sim 1260\text{ cm}^{-1}$) and amide I ($\sim 1680\text{ cm}^{-1}$) peaks, which arise largely from the collagen [37], and the CH_2 peak which is present in both collagenous and non-collagenous organic molecules. Bone is laid down in lamellae, in both cortical and trabecular bone, and within each lamella collagen fibrils are partially aligned with the direction of preferred orientation usually at angle to the bone or trabecular axis [2]. The triple helical arrangement of the collagen molecule constrains the positions of the amide bonds with respect to the

molecular axis. Within this bond the chemical groups contributing to the Amide I band (predominantly C=O) lie in a plane perpendicular to the molecular axis, while those contributing to the Amide III band (mostly C-N) are both perpendicular and along this axis. Mineral crystals are found within the collagen matrix with their crystallographic *c*-axis aligned with the collagen fibres [2]. It has been shown that the maximum Raman signal is produced when the polarisation of the exciting radiation is parallel with this axis [38].

Our experimental arrangement may result in trabecular samples having a preferred orientation with respect to the incident laser beam. This factor can influence the intensity of a Raman signal in addition to any compositional affect. We have used a method derived from the published literature [39] to reduce the effect of orientation so we could attribute any difference between readings from cortical and trabecular bone to differences in composition. The intensity of the phosphate ν_4 peak was taken as an indicator of mineral content, in preference to any of the other phosphate bands, as it has been shown to be less susceptible to orientation effects [39] and as an asymmetric bend it is less affected by polarisation [40]. For similar reasons the Amide III peak was used as a measure of collagen content [39]. The mineral to matrix ratio was calculated from the intensity of the phosphate ν_4 (mineral) peak divided by Amide III (matrix) peak. While the peak at 1070 cm^{-1} is a formed by contributions from both carbonate and phosphate ν_3 , it has been shown to be a good measure of the carbonate content of bone [58]. The carbonate to phosphate ratio was, therefore, calculated by dividing the value from the carbonate peak (1070 cm^{-1}) by the phosphate ν_4 peak and the relative amount of HPO_4^{2-} by dividing the amplitude of this peak (1003 cm^{-1}) by that of the phosphate ν_4 peak [37]. Values for the intensity of the carbonate and HPO_4^{2-} peaks were found by curve fitting to remove any possible contribution from the phosphate ν_1 (960 cm^{-1}) and ν_3 (1040 cm^{-1}) bands. Two peaks can be fitted to the Amide I band, each indicative of a different secondary structure within the collagen matrix. The ratio of these two peaks gives an

indication of the abundance of each structure. In FTIR spectroscopy, this ratio has been shown to give a measure of mature, trivalent bonds compared with the immature, divalent variety [41] while others have used it to show the change in collagen structure following loading beyond the yield point in a Raman experiment [20]. As bone matures so the size of the individual mineral crystals increases, contributing to a narrower, more intense ν_1 peak, while at the same time increased substitutions into the crystal lattice by carbonate and other ions reduce the purity of the crystal so reducing the peak height and increasing its width. The full width at half maximum height of this peak taken together with the degree of substitution values (carbonate to phosphate ratio) give an indication of the degree of crystallinity of the mineral part of the bone [42].

Principal component analysis

Spectra were presented for PCA following background subtraction and removal of wavenumbers with an average intensity remaining of less than 100 counts. Deleting these regions has no effect on peaks associated with bone. The components or variables generated from the PCA are common to femur and tibia as well as cortical and trabecular bone. After reference to a scree plot [43] scores for the first 6 coefficients from cortical and trabecular bone were then compared using Student's *t*-test as described below.

Statistics

Data were found to be normally distributed ($P > 0.05$ from Kolmogorov-Smirnov test) so mean values from each parameter were compared using 2-way ANOVA using bone type (cortical/trabecular) and sample origin (femur/tibia) as the two independent variables. No interaction was found between these variables so results from femur and tibia were analyzed separately using Student's *t*-tests. Due to the different number of spectra recorded from each sample a weighted comparison of means was used to calculate the *P*-value [44]. Results were

considered significant if $P < 0.05$. A custom script was written in Matlab (R2006b, the MathWorks, Inc) to perform t -tests and Sigmastat (Version 3.5, Systat Software Inc.) was used for other tests.

Results

Difference spectra

Plots of the average spectra from cortical and trabecular bone from femur and tibia are shown together with their difference (Figure 2). For the femur the intensity of the signal coming from trabecular bone (maximum ν_1 7400) was larger than that from the cortex (maximum ν_1 5800) (Figure 2A) and the difference was negative over the whole spectrum (Figure 2E). This difference was not statistically significant in any regions corresponding to major peaks (Figure 2B). In the tibia this pattern was reversed; trabecular bone had a maximum signal for ν_1 of 9900 compared with ν_1 of 16200 from the cortical bone (Figure 2C), so the difference was positive (Figure 2E). Overall, the magnitude of the difference in the tibia was about 3 times that seen in the femur and was significant ($P < 0.05$) at almost all wave numbers (Figure 2D).

Peak parameters

The mineral to matrix ratio (phosphate ν_4 /Amide III) was significantly greater in cortical bone than in trabecular bone for both the femur ($P=0.001$) and the tibia ($P=0.002$) (Figures 3A and 3B, respectively). The carbonate to phosphate ratio was also greater in cortical than trabecular bone (Figure 4). The difference was significant in tibia ($P < 0.001$), while in femur the significance reached $P=0.054$, marginally outside the traditional threshold. The ratio of hydrogen phosphate to phosphate was bigger in trabecular bone in both femur and tibia although the difference was not significant (Figure 5). There were no significant differences in the ratio of intensities of peaks fitted within the amide I band (Figure 6) or the FWHM of

the phosphate ν_1 peak (Figure 7) between cortical and trabecular bone, in either the femur or the tibia.

PCA

The first principal component (PC) (Figure 8) accounted for 99% of the variance within the data. It corresponds very closely with a Raman spectrum from bone. Scores from this component from cortical and trabecular bone were significantly different in tibia (25200 and -900, $P=0.01$) but not in femur (-16800 and -10500, $P=0.27$).

Average scores for PCs 2-6 are displayed in Figure 9. Scores for PCs 2 and 3 for trabecular bone were positive and significantly ($P<0.01$) different from those from cortical bone, which were negative, in both femur and tibia. The position was reversed for PCs 5 and 6 where the scores for trabecular bone were negative while those from cortical bone were positive, although this difference was only significant ($P<0.05$) in tibia but not in femur. The PCs mentioned are plotted in Figure 10 below and show where the main differences lie in relation to a typical bone spectrum.

Discussion

Raman microscopy has been used to investigate the differences in bone chemistry between cortical and trabecular bone from C57Bl6 mice. Our results show the bone types are different, with cortical bone being more mineralized and with a greater carbonate content. These differences are consistent with cortical bone appearing “older” than trabecular material [45] as traditionally believed from other studies of bone turnover (refs?)

The laser used for Raman excitation is linearly polarised. In addition, bone contains lamellae which themselves contain oriented collagen fibres and mineral crystallites. This means that many of the Raman bands are sensitive to the orientation of the sample with respect to the

polarisation of the beam. This has been almost unrecognised in the mineralised tissue literature in spite of many publications investigating bone composition using a similar experimental arrangement to ours. Because we recognised this issue late in our experimental work and had not included polarising optics in the beam path, we tried to take steps to minimise the effects by selecting bands that are reported to be least sensitive to polarisation [39]. This is a complicated problem and a full treatment is beyond the scope of this article.

Difference

The intensity of a Raman signal is primarily due to the number of scattering centres excited within the sample [46,47]. This can be affected by a number of factors including the orientation of the molecules with respect to a polarised incident beam [39], the mode of molecular vibration [40], and the presence of other atoms or scattering centres, though each of these is likely to affect particular bands in the spectrum.

With the experimental arrangement used in this study, the sampling volume was full of bone in all cases and care was taken to ensure that the laser intensity remained constant, as judged by the silicon standard. If, therefore, the bone material was the same in all cases, a similar signal intensity from both cortical and trabecular bone and from tibia and femur would be expected. Having taken these precautions in the recording of the spectra, normalisation of the spectra was not undertaken in order to obtain a direct measure of the composition of the bone matrix in each type of bone in each of the femur and tibia.

The measured intensities and difference spectra above show some unexpected results: a significantly larger signal was obtained from both the cortical and trabecular bone from the tibia than the femur, with the biggest difference being found in cortical bone in which approximately 3 times the signal was measured from the tibia than from the femur. Signal

from trabecular bone was similar in both femur and tibia. In the femur, the cortical signal was slightly, but not significantly, smaller than that from trabecular bone, whereas in the tibia this was reversed, with cortical bone yielding a much higher signal. Some of the difference may be due to the different loading regimes experienced by the two bones (new ref?), although there are likely to be other factors which are currently under investigation.

Band intensity parameters

Mineralization of the collagen matrix is reported to be a two stage process occurring outside the osteoblast. An initial mineralisation phase of a few months is followed by a longer more gradual phase resulting in fully mineralised bone [4]. As the mineralisation process proceeds so the chemistry of the mineral alters with the carbonate content increasing and the monohydrogen phosphate (HPO_4^{2-}) content decreasing [45,48]. An assessment of the relative amounts of these materials - mineral to matrix ratio, carbonate to phosphate ratio, HPO_4^{2-} to phosphate ratio – would give an indication of the age of the bone being investigated. The intensity of any of the three phosphate peaks have been used widely as indicators of mineral content in bone, while the Amide I or III bands are markers of collagen [20,37,49,50] (see Figure 1 above). We have selected the phosphate ν_4 mode and the Amide III band because of their insensitivity to orientation and polarisation effects [39,40]. The carbonate ion is a natural part of bone mineral, substituting for hydroxide (A-type) and phosphate (B-type) [51,52]. Both types can be detected in a Raman spectrum of bone with B-type producing a band at $\sim 1070 \text{ cm}^{-1}$ and the A type a weak shoulder at $\sim 1104 \text{ cm}^{-1}$ [28] (see Figure 1). We have used the B-type substitution as an indicator of carbonate content because of its association with aging [45,48]. Our measure of mineral to matrix ratio shows cortical bone was more mineralised than trabecular material, in agreement with other studies [11-13]. Taken with the higher carbonate to phosphate ratio and lower HPO_4^{2-} to phosphate ratio we found in cortical

bone these results suggest cortical bone is older than trabecular material, a finding consistent with the lower turnover of bone observed in the cortical compartment [53].

Comparing the intensity of the profiles fitted within the main bands of a Raman spectrum yields further information about the nature of the collagen and mineral within the sample. For example, the ratio of two profiles centred at 1670 and 1690 cm^{-1} fitted within the Amide I band in an FTIR spectrum gives a measure of the degree of collagen cross-linking in the bone [41] with an increase in the ratio indicative of a greater proportion of mature or trivalent cross-links. Other authors have also used this measure in Raman spectroscopy [22,54,55] although this has never been shown experimentally, so it is probably more accurate to attribute the two peaks to different collagen secondary structures. Our investigation showed no differences in the organisation of the mineral or matrix compartments of bone from cortical and trabecular regions.

PCA

PCA assesses intensities at all wavenumbers simultaneously and generates ordered components or variables that account for the variance within the data analysed. The first few components describe the majority of the variance and so can be used instead of the original variables (wavenumbers in this case) to analyse the data. Typically, of the order of ten new variables, the modes of variation or principal components, are used to replace the vast number of original variables. Due to the nature of PCA these new variables are orthogonal, or independent. Each mode is assigned a score that describes the spectrum from each sample and this smaller number of variables can be treated as any other data.

In this study, Coefficient 1 is very similar to a typical Raman spectrum from bone and the score represents a signal magnitude for each sample. This arises because the data are not

normalised during analysis as described above. 99% of the variance is explained by this variable indicating signal strength is the biggest difference between individual measurements.

As can be seen in Figure 10, the Amide I band is the only complete band seen in PC2. Adjacent positive and negative peaks seen in the phosphate ν_1 , ν_2 and ν_4 bands are suggestive of peak wavenumber shifts or changes in relative intensities of sub bands. Analysis of profile centres indicates that sub-bands from cortical bone occur at a slightly higher wavenumbers than corresponding sub-bands from trabecular bone. A similar finding was made when measuring the effect of compression on bone using Raman microscopy [56]. This may suggest cortical bone is preloaded, possibly as a form of protection against excessive loads, in a similar way to wood in the trunk of trees [57].

PC3 has bands coinciding with those arising from collagen in bone. An inverted carbonate peak is also seen along with a negative spike centred at about 954 cm^{-1} , usually assigned to a carbonate substituted apatite [48] or octacalcium phosphate (OCP) [24]. This coefficient could be thought of as an inverse mineral: matrix ratio and as the scores from trabecular bone are higher (see Figure 9) would suggest the mineral: matrix ratio is lower in trabecular bone. This is in agreement with the mineral: matrix ratio derived from individual peaks (see Figure 3).

Coefficients 5 and 6 are very similar with negative portions in the phosphate ν_2 and ν_4 and amide I regions and positive sections in proline ($840\text{-}900\text{ cm}^{-1}$), B type carbonate, Amide III and CH_2 bands. The major difference is in the phosphate ν_1 band where the adjacent positive and negative peaks are inverted between the two PCs. Unsurprisingly, the scores from these PCs are similar in each sample.

Taken together, these results show there are differences in the Raman scattering between cortical and trabecular bone from the mice examined in this paper, reflecting differences

found using other techniques. Cortical bone appears “older” than trabecular bone and this could arise from the lower turnover generally reported in cortical bone [4]. The different signals found between femoral and tibial bone were a surprise, as was also the inversion of the ratio of cortical to trabecular signal in going from femur to tibia. Further studies are underway to try to understand the origins of these results.

References

- [1] Cowin SC. Bone mechanics handbook. Boca Raton, FL: CRC Press; 2001:
- [2] Rho J-, Kuhn-Spearing L, Zioupos P. Mechanical properties and the hierarchical structure of bone. *Medical Engineering and Physics* 1998;20:92-102.
- [3] Bianco P, Gehron Robey P. Marrow stromal stem cells. *J Clin Invest* 2000;105:1663-8.
- [4] Favus MJ, American Society for Bone and Mineral Research. Primer on the metabolic bone diseases and disorders of mineral metabolism. Philadelphia ; London: Lippincott Williams & Wilkins; 1999:502.
- [5] Warner SE, Shea JE, Miller SC, Shaw JM. Adaptations in cortical and trabecular bone in response to mechanical loading with and without weight bearing. *Calcified Tissue International* 2006;79:395-403.
- [6] - , Benhamou C-, Courteix D. Short-term and long-term site-specific effects of tennis playing on trabecular and cortical bone at the distal radius. *Journal of Bone and Mineral Metabolism* 2006;24:484-90.
- [7] Michalsky M, Norrissuarez K, Bettica P, Pecile A, Moro L. Rat cortical and trabecular bone collagen glycosylation are differently influenced by ovariectomy. *Biochemical and Biophysical Research Communications* 1993;192:1281-8.
- [8] Morko J, Kiviranta R, Hurme S, Rantakokko J, Vuorio E. Differential turnover of cortical and trabecular bone in transgenic mice overexpressing cathepsin K. *Bone* 2005;36:854-65.
- [9] Duan Y, De Luca V, Seeman E. Parathyroid hormone deficiency and excess: Similar effects on trabecular bone but differing effects on cortical bone. *Journal of Clinical Endocrinology and Metabolism* 1999;84:718-22.

- [10] Genant HK, Guglielmi G, Jergas M. Bone densitometry and osteoporosis. Berlin ; New York: Springer; 1998:602.
- [11] Gong JK, Arnold JS, Cohn SH. Composition of trabecular and cortical bone. *Anat Rec* 1964;149:325-31.
- [12] Mulder L, Koolstra JH, De Jonge HW, Van Eijden TMGJ. Architecture and mineralization of developing cortical and trabecular bone of the mandible. *Anatomy and Embryology* 2006;211:71-8.
- [13] Bigi A, Cojazzi G, Panzavolta S, et al. Chemical and structural characterization of the mineral phase from cortical and trabecular bone. *Journal of Inorganic Biochemistry* 1997;68:45-51.
- [14] NorisSuarez K, Romanello M, Bettica P, Moro L. Collagen type I of rat cortical and trabecular bone differs in the extent of posttranslational modifications. *Calcified Tissue International* 1996;58:65-9.
- [15] Zysset PK, Edward Guo X, Edward Hoffler C, Moore KE, Goldstein SA. Elastic modulus and hardness of cortical and trabecular bone lamellae measured by nanoindentation in the human femur. *Journal of Biomechanics* 1999;32:1005-12.
- [16] Rho J-, Tsui TY, Pharr GM. Elastic properties of human cortical and trabecular lamellar bone measured by nanoindentation. *Biomaterials* 1997;18:1325-30.
- [17] Bumrerraj S, Katz JL. Scanning acoustic microscopy study of human cortical and trabecular bone. *Annals of Biomedical Engineering* 2001;29:1034-42.

[18] Turner CH, Rho J, Takano Y, Tsui TY, Pharr GM. The elastic properties of trabecular and cortical bone tissues are similar: Results from two microscopic measurement techniques. *Journal of Biomechanics* 1999;32:437-41.

[19] Bayraktar HH, Morgan EF, Niebur GL, Morris GE, Wong EK, Keaveny TM. Comparison of the elastic and yield properties of human femoral trabecular and cortical bone tissue. *Journal of Biomechanics* 2004;37:27-35.

[20] Carden A, Rajachar RM, Morris MD, Kohn DH. Ultrastructural changes accompanying the mechanical deformation of bone tissue: A raman imaging study. *Calcified Tissue International* 2003;72:166-75.

[21] Crane NJ, Morris MD, Ignelzi Jr. MA, Yu G. Raman imaging demonstrates FGF2-induced craniosynostosis in mouse calvaria. *Journal of Biomedical Optics* 2005;10:1-8.

[22] Dehring KA, Crane NJ, Smukler AR, McHugh JB, Roessler BJ, Morris MD. Identifying chemical changes in subchondral bone taken from murine knee joints using raman spectroscopy. *Applied Spectroscopy* 2006;60:1134-41.

[23] Dehring KA, Smukler AR, Roessler BJ, Morris MD. Correlating changes in collagen secondary structure with aging and defective type II collagen by raman spectroscopy. *Applied Spectroscopy* 2006;60:366-72.

[24] Crane NJ, Popescu V, Morris MD, Steenhuis P, Ignelzi Jr. MA. Raman spectroscopic evidence for octacalcium phosphate and other transient mineral species deposited during intramembranous mineralization. *Bone* 2006;39:434-42.

- [25] Kozloff KM, Carden A, Bergwitz C, et al. Brittle IV mouse model for osteogenesis imperfecta IV demonstrates postpubertal adaptations to improve whole bone strength. *Journal of Bone and Mineral Research* 2004;19:614-22.
- [26] Silva MJ, Brodt MD, Wopenka B, et al. Decreased collagen organization and content are associated with reduced strength of demineralized and intact bone in the SAMP6 mouse. *Journal of Bone and Mineral Research* 2006;21:78-88.
- [27] Redey SA, Nardin M, Bernache-Assolant D, et al. Behavior of human osteoblastic cells on stoichiometric hydroxyapatite and type A carbonate apatite: Role of surface energy. *Journal of Biomedical Materials Research* 2000;50:353-64.
- [28] Penel G, Delfosse C, Descamps M, Leroy G. Composition of bone and apatitic biomaterials as revealed by intravital raman microspectroscopy. *Bone* 2005;36:893-901.
- [29] Ager JW, Nalla RK, Breedon KL, Ritchie RO. Deep-ultraviolet raman spectroscopy study of the effect of aging on human cortical bone. *Journal of Biomedical Optics* 2005;10:1-8.
- [30] Akkus O, Adar F, Schaffler MB. Age-related changes in physicochemical properties of mineral crystals are related to impaired mechanical function of cortical bone. *Bone* 2004;34:443-53.
- [31] Hofmann T, Heyroth F, Meinhard H, Franzel W, Raum K. Assessment of composition and anisotropic elastic properties of secondary osteon lamellae. *Journal of Biomechanics* 2006;39:2282-94.
- [32] Kazanci M, Wagner HD, Manjubala NI, et al. Raman imaging of two orthogonal planes within cortical bone. *Bone* 2007;41:456-61.

- [33] Somerville JM, Aspden RM, Armour KE, Armour KJ, Reid DM. Growth of C57Bl/6 mice and the material and mechanical properties of cortical bone from the tibia. *Calcified Tissue International* 2004;74:469-75.
- [34] Cai TT, Zhang D, Ben-Amotz D. Enhanced chemical classification of raman images using multiresolution wavelet transformation. *Applied Spectroscopy* 2001;55:1124-30.
- [35] Barclay VJ, Bonner RF, Hamilton IP. Application of wavelet transforms to experimental spectra: Smoothing, denoising, and data set compression. *Analytical Chemistry* 1997;69:78-90.
- [36] Lieber CA, Mahadevan-Jansen A. Automated method for subtraction of fluorescence from biological raman spectra. *Applied Spectroscopy* 2003;57:1363-7.
- [37] Timlin JA, Carden A, Morris MD. Chemical microstructure of cortical bone probed by raman transects. *Applied Spectroscopy* 1999;53:1429-35.
- [38] Tsuda H, Arends J. Orientational micro-raman spectroscopy on hydroxyapatite single crystals and human enamel crystallites. *Journal of Dental Research* 1994;73:1703-10.
- [39] Kazanci M, Roschger P, Paschalis EP, Klaushofer K, Fratzl P. Bone osteonal tissues by raman spectral mapping: Orientation-composition. *J Struct Biol* 2006;156:489-96.
- [40] Banwell CN, McCash EM. *Fundamentals of molecular spectroscopy*. London ; New York: McGraw-Hill; 1994:308.
- [41] Paschalis EP, Verdelis K, Doty SB, Boskey AL, Mendelsohn R, Yamauchi M. Spectroscopic characterization of collagen cross-links in bone. *Journal of Bone and Mineral Research* 2001;16:1821-8.

- [42] Freeman JJ, Wopenka B, Silva MJ, Pasteris JD. Raman spectroscopic detection of changes in bioapatite in mouse femora as a function of age and in vitro fluoride treatment. *Calcified Tissue International* 2001;68:156-62.
- [43] Hair JF. *Multivariate data analysis*. Upper Saddle River, N.J.: Prentice Hall; 1998:
- [44] Bland JM, Kerry SM. Statistics notes: Weighted comparison of means. *British Medical Journal* 1998;316:129.
- [45] Akkus O, Polyakova-Akkus A, Adar F, Schaffler MB. Aging of microstructural compartments in human compact bone. *Journal of Bone and Mineral Research* 2003;18:1012-9.
- [46] Smith E. *Modern raman spectroscopy : A practical approach*. Chichester: John Wiley; 2005:210.
- [47] Baranska H. *Laser raman spectrometry : Analytical applications*. Horwood; 1987:
- [48] Tarnowski CP, Ignelzi Jr. MA, Morris MD. Mineralization of developing mouse calvaria as revealed by raman microspectroscopy. *Journal of Bone and Mineral Research* 2002;17:1118-26.
- [49] Timlin JA, Carden A, Morris MD, et al. Spatial distribution of phosphate species in mature and newly generated mammalian bone by hyperspectral raman imaging. *Journal of Biomedical Optics* 1999;4:28-34.
- [50] Morris MD, Finney WF. Recent developments in raman and infrared spectroscopy and imaging of bone tissue. *Spectroscopy* 2004;18:155-9.

[51] Mkukuma LD, Skakle JMS, Gibson IR, Imrie CT, Aspden RM, Hukins DWL. Effect of the proportion of organic material in bone on thermal decomposition of bone mineral: An investigation of a variety of bones from different species using thermogravimetric analysis coupled to mass spectrometry, high-temperature X-ray diffraction, and fourier transform infrared spectroscopy. *Calcified Tissue International* 2004;75:321-8.

. Human tooth enamel: A raman polarized approach. *Applied Spectroscopy* 2002;56:1030-4.

[53] Ferguson N. *Osteoporosis in focus*. London: Pharmaceutical Press; 2004:229.

[54] Pelton JT, McLean LR. Spectroscopic methods for analysis of protein secondary structure. *Analytical Biochemistry* 2000;277:167-76.

[55] Chi Z, Chen XG, Holtz JSW, Asher SA. Uv resonance raman-selective amide vibrational enhancement: Quantitative methodology for determining protein secondary structure. *Biochemistry* 1998;37:2854-64.

[56] De Carmejane O, Morris MD, Davis MK, et al. Bone chemical structure response to mechanical stress studied by high pressure raman spectroscopy. *Calcified Tissue International* 2005;76:207-13.

[57] Burgert I, Eder M, Gierlinger N, Fratzl P. Tensile and compressive stresses in tracheids are induced by swelling based on geometrical constraints of the wood cell. *Planta* 2007;226:981-7.

[58] Awonusi A, Morris MD, Tecklenburg MMJ. Carbonate assignment and calibration in the raman spectrum of apatite. *Calcified Tissue International* 2007;81:46-52.

Acknowledgements

The authors would like to thank the BBSRC for funding of the Raman microscope (BBC5125101), the College of Life Sciences and Medicine and the College of Physical Sciences at the University of Aberdeen for funding of a studentship (SG) and Dr R. J. Van'T Hof of the University of Edinburgh for providing the mouse bone.

Figure Legends

Figure 1

A typical Raman spectrum from bone showing the major peaks and their molecular origins. Background signal has been removed.

Figure 2

Average spectra from cortical and trabecular bone from femur (A) and tibia (B) and their differences (E). Wavenumbers where the differences are significant are plotted in the right hand panels (B and D).

Figure 3

The mineral to matrix ratio showing the comparison between cortical and trabecular bone from femur (A) and tibia (B).

Figure 4

Carbonate to phosphate ratio showing the comparison between cortical and trabecular bone from femur (A) and tibia (B).

Figure 5

Hydrogen phosphate (HPO_4^{2-}) to phosphate ratio showing the comparison between cortical and trabecular bone from femur (A) and tibia (B).

Figure 6

Ratio of intensities of peaks centred at 1670 and 1690 cm^{-1} , fitted within the Amide I band, indicating different secondary structures in the collagen matrix (femur (A) and tibia (B)).

Figure 7

Mineral crystallinity measured by the FWHM of the phosphate ν_1 peak. A narrower peak is indicative of purer mineral with larger crystal (femur (A) and tibia (B)).

Figure 8

PCA component 1. Coefficient 1 from the PCA accounts for 99% of the variance and represents a magnitude effect. This is present because data were not normalised. Note the similarity to the spectrum from bone plotted in Figure 1.

Figure 9

PCA scores for coefficients 2-6 for femur (A) and tibia (B). a - $P < 0.01$, b - $P < 0.05$.

Figure 10

PCA components with a significant difference between cortical and trabecular bone. Coefficients 2 and 3 (A and B) were significantly different in femur and tibia while coefficients 5 and 6 (C and D) were significantly different in tibia only. Vertical lines mark the position of peak maxima in a typical Raman spectrum from bone.

Fig 1

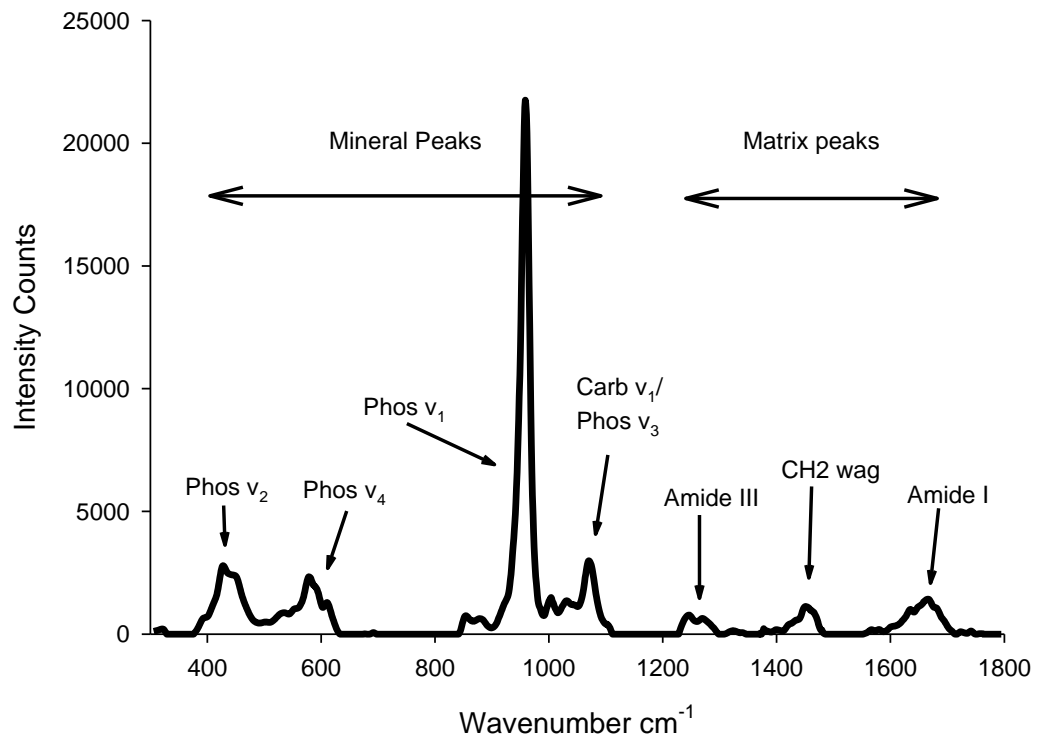


Fig 2

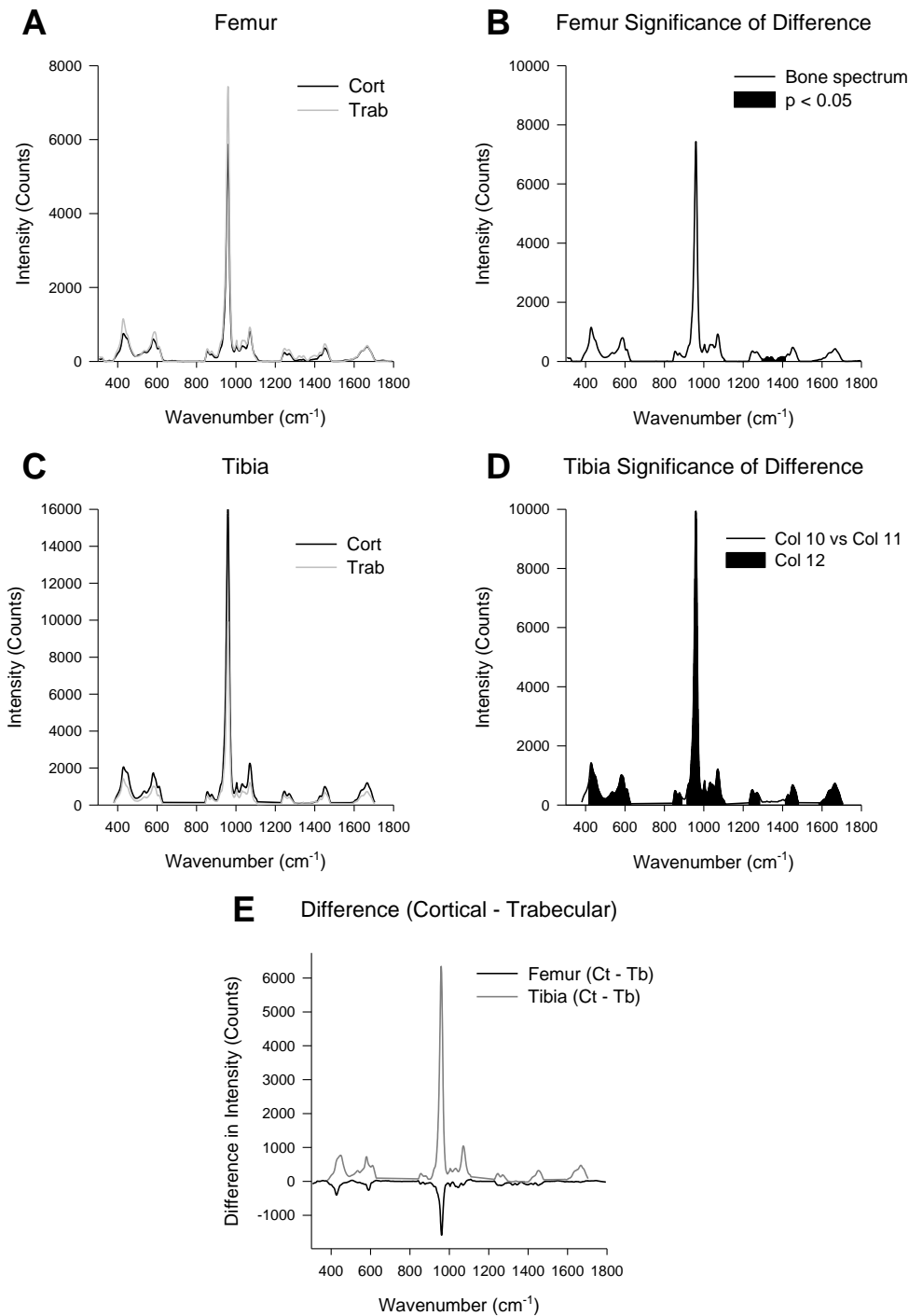


Fig 3

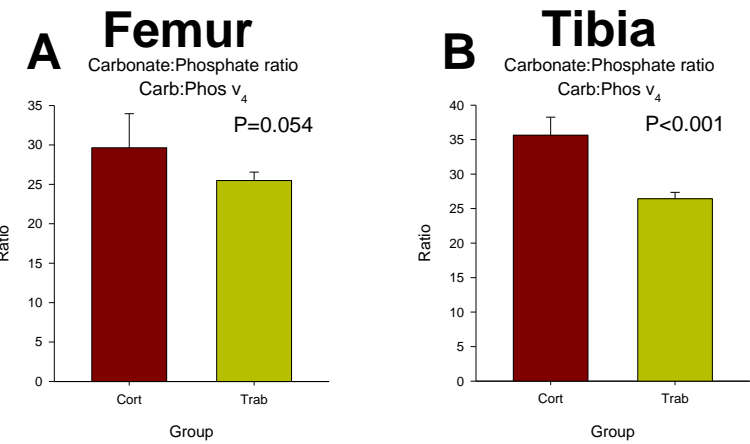
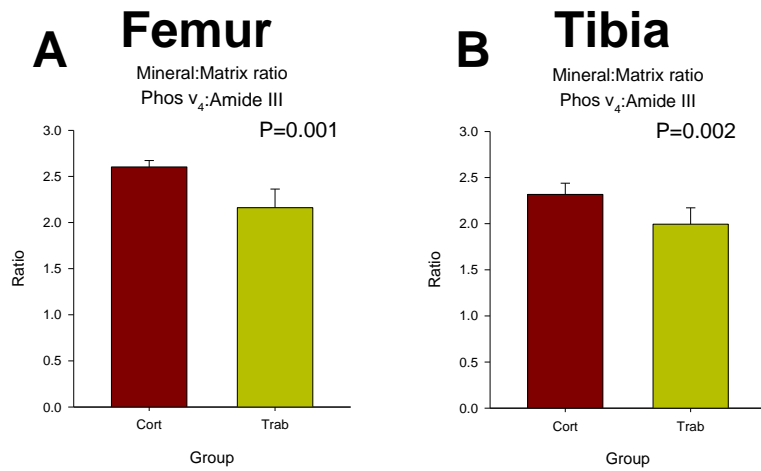


Fig 4

Fig 5

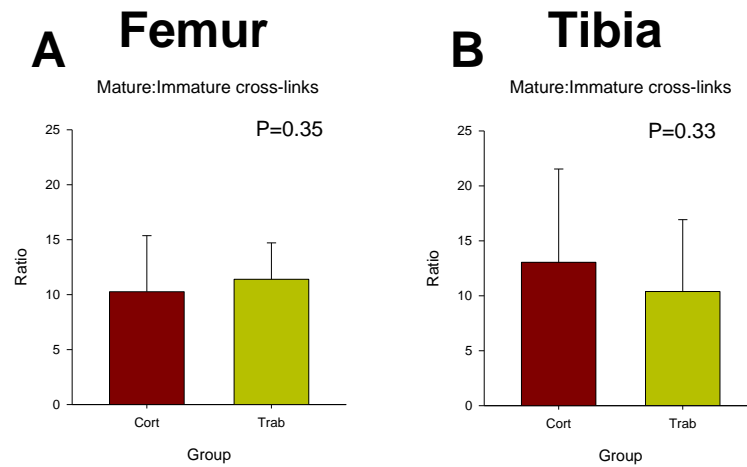
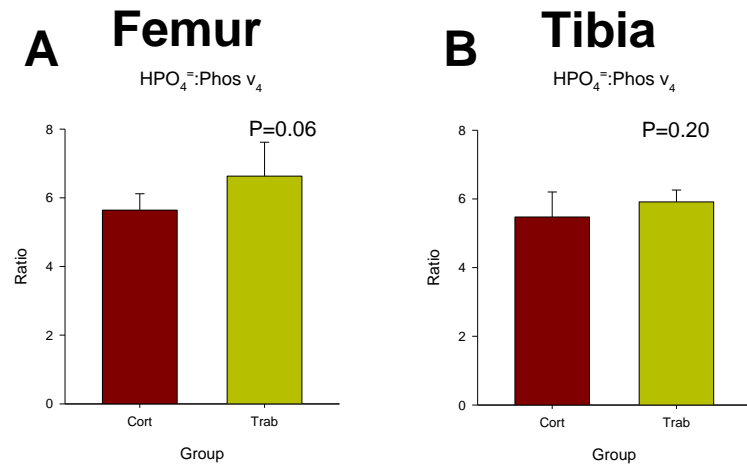
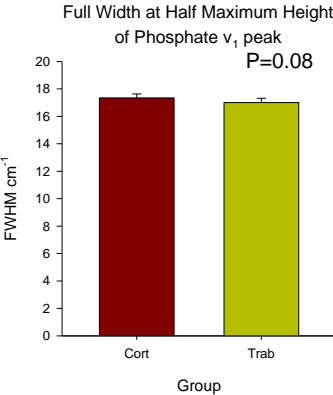


Fig 6

Fig 7

A Femur



B Tibia

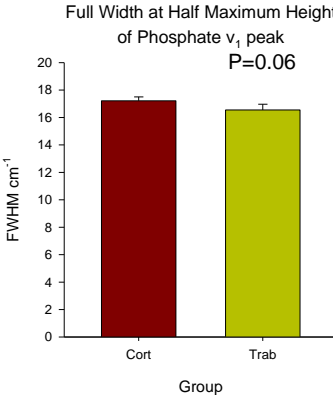


Fig 8

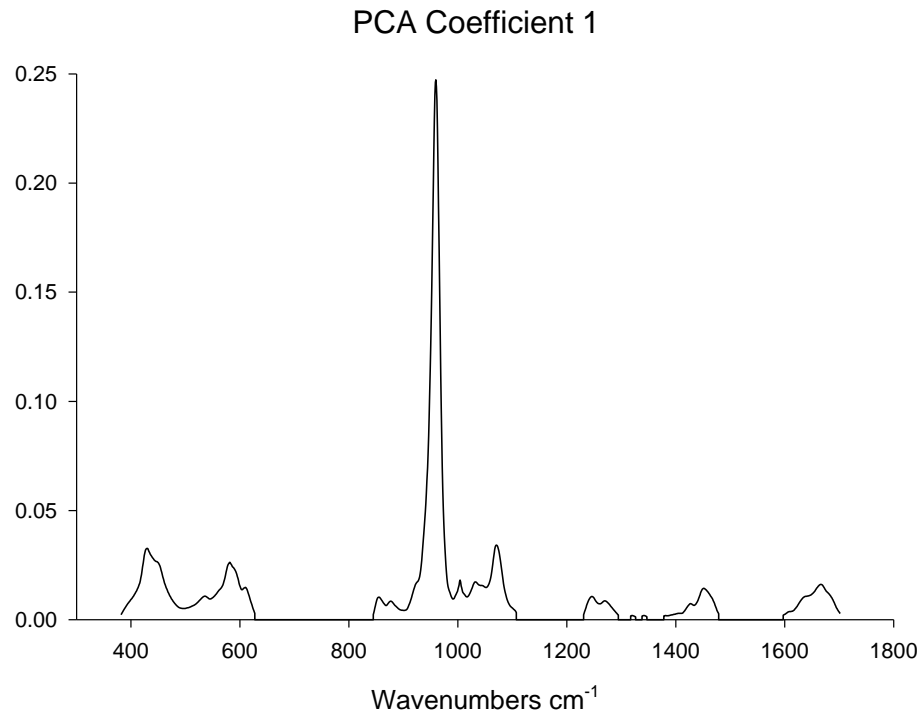


Fig 9

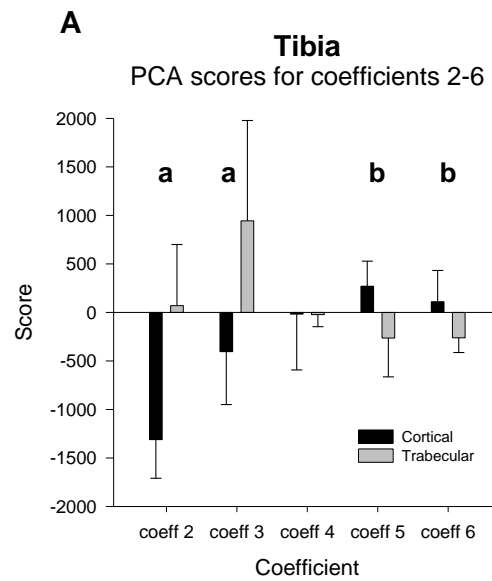
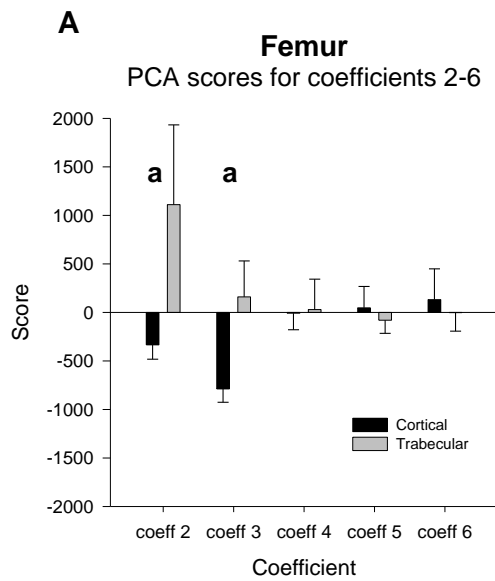


Fig 10

